Geometry optimization of a double-layered inertial reactive armor configured with rotating discs

Bekzat Ajan[2], Dichuan Zhang[*1], Christos Spitas[2],
Elias Abou Fakhr[2] and Dongming Wei[3]

*[1]Department of Civil and Environmental Engineering, School of Engineering and Digital Sciences,
Nazarbayev University, Astana 010000, Kazakhstan*
*[2]Department of Mechanical and Aerospace Engineering, School of Engineering and Digital Sciences,
Nazarbayev University, Astana 010000, Kazakhstan*
*[3]Department of Mathematics, School of Sciences and Humanities,
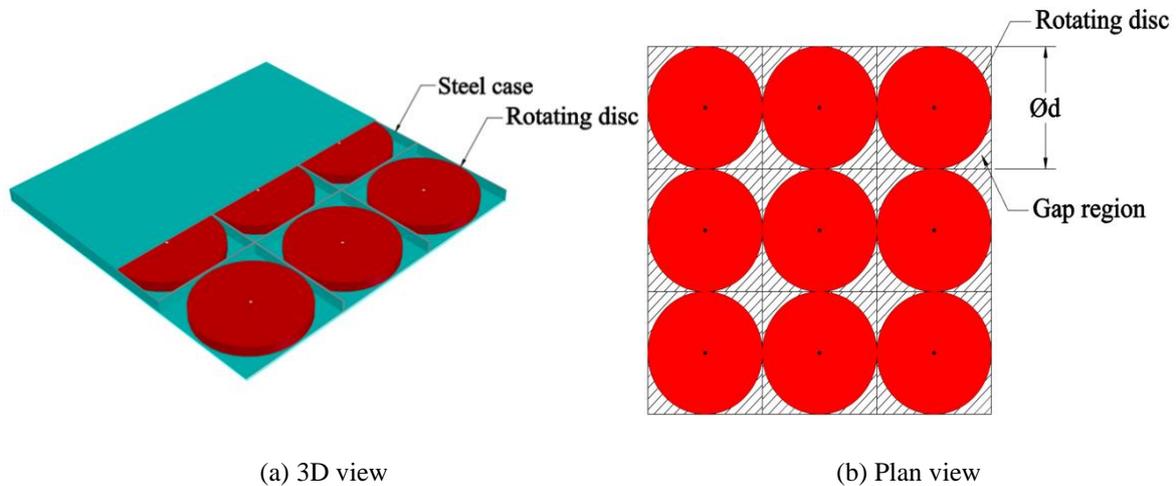Nazarbayev University, Astana 010000, Kazakhstan*

Abstract.   An innovative inertial reactive armor is being developed through a multi-discipline project. Unlike the well-known explosive or non-explosive reactive armour that uses high-energy explosives or bulging effect, the proposed inertial reactive armour uses active disc elements that is set to rotate rapidly upon impact to effectively deflect and disrupt shaped charges and kinetic energy penetrators. The effectiveness of the proposed armour highly depends on the tangential velocity of the impact point on the rotating disc. However, for a single layer armour with an array of high-speed rotating discs, the tangential velocity is relatively low near the center of the disc and is not available between the gap of the discs. Therefore, it is necessary to configure the armor with double layers to increase the tangential velocity at the point of impact. This paper explores a multi-objective geometry design optimization for the double-layered armor using Nelder-Mead optimization algorithm and integration tools of the python programming language. The optimization objectives include maximizing both average tangential velocity and high tangential velocity areas and minimizing low tangential velocity area. The design parameters include the relative position (translation and rotation) of the disc element between two armor layers. The optimized design results in a significant increase of the average tangential velocity (38%), increase of the high tangential velocity area (71.3%), and decrease of the low tangential velocity area (86.2%) as comparing to the single layer armor.

Keywords: double-layered armor; geometry design; inertial reactive armor; multi-objective optimization

1. Introduction

Reactive armor is a supplementary form of armor that has been developed to minimize the impact of highly energetic projectiles on primary armor by exhibiting specific reactions upon impact. These projectiles include shaped charge explosives and kinetic energy penetrators (KEP) (Graswald *et al.* 2019). To achieve high kinetic energy, these projectiles are designed with minimized diameter, maximized mass through increased length, and utilize dense materials like

---

∗Corresponding author, Professor, E-mail: dichuan.zhang@nu.edu.kz

(a) 3D view   (b) Plan view

Fig. 1 Single layer IRA schematic view

depleted uranium and tungsten heavy alloys. Furthermore, they are accelerated to approximately 1500 m/s at the moment of impact (Lanz *et al*. 2001). Passive armor alone cannot withstand the immense amount of kinetic energy concentrated in a small area. However, the invention of two types of reactive armor, namely Explosive Reactive Armor (Mayseless 2011) and Non-Explosive Reactive Armor (NERA) (Fras 2021a), has significantly enhanced the armor's ability to neutralize incoming projectiles. The underlying mechanism of these armor systems revolves around reducing the kinetic energy of the impacting projectile through various asymmetrical forces, such as deceleration, fragmentation, erosion, and deflection, before it reaches the primary armor (Rosenberg *et al*. 2008).

A multidisciplinary project is currently underway to develop an innovative inertial reactive armor (IRA) with the objective of safeguarding military vehicles against kinetic projectiles and molten metal jets. In contrast to conventional reactive armor that relies on high-energy explosives (e.g., ERA) or bulging effects (e.g., NERA), the proposed IRA employs active disc elements designed to rapidly rotate upon impact. This rotational motion aims to effectively deflect and disrupt highly energetic penetrators by inducing transverse inertial exchange, thereby causing them to buckle rapidly.

The proposed IRA possesses several notable advantages over existing reactive armor technologies. Firstly, it exhibits a thinner and more compact profile, contributing to reduced weight and improved vehicle maneuverability. Despite its streamlined design, the IRA maintains superior protective capabilities regardless of the angle of incidence of the penetrator.

An example layout of the IRA with an array of the discs is shown in Fig.1. Each disc is enclosed in a steel case. The activation of the rotation of each disc can be done through a small detonation inside the disc. As follows from the basic physics of ballistics, the effectiveness of the proposed IRA is highly dependent on the tangential velocity of the rotating disc at the point of impact. However, for a single layer armor with an array of high-speed rotating discs, the tangential velocity is relatively low near the center of the disc and is not available in gap regions inside the steel case and between adjacent discs (see Fig. 1b).

Therefore, a double-layer solution with translation offsetting and rotation between each layer is proposed in this paper to maximize the tangential velocity at the point of impact. Geometry optimization is a process of designing and refining the shape and structure of a material or system to improve its performance. In the context of double-layered inertial reactive armor configured with rotating discs, geometry optimization aims to improve its effectiveness of deflection and disruption of penetrators by maximizing the tangential velocity at the point of the impact.

The optimization can be done by displace and/or rotate the 2nd layer from the 1st layer of the discs. This paper explores a multi-objective geometry optimization of the double-layered armor using Nelder–Mead method (Boorla *et al*. 2019) (Gordini *et al*. 2017). At a given rotation speed, three objectives were used for optimization. The three objectives are: (1) maximizing average tangential velocity over the entire protection area; (2) maximizing high tangential velocity area, and (3) minimizing low tangential velocity area. To achieve these objectives, the relative position varied through translation and rotation between two armor layers.

2. Background

2.1 Reactive armor

Two types of reactive armor have been developed including explosive and non-explosive reactive armor (Cohen-Arazi *et al*. 2012, Held 1973). The explosive reactive armor (ERA) consists of a high-energy explosive layer sandwiched by two steel plates (cassettes). The explosive layer detonation moves the plates to the sides at the moment of impact of the armor with the projectile, which can destabilize and destroy the projectile, preventing it from interacting with the main armor (Mayseless 1984, Mayseless 2011, Mayseless *et al*. 2019). The effectiveness of ERA depends on the geometry parameters such as: obliquity angle to the projectile, thickness of plates, and non-geometry parameters: velocity and material of the plates. Liden *et al*. studied experimental interaction of moving plates with a tungsten long-rod projectile, similar to the mechanism of ERA.

They conducted experiments followed by simulations varying the values of plates thickness 0.5d, d and 2d, where d is the diameter of the hitting projectile, and the obliquity angle 30º, 60º and 70º against a projectile hitting at 1500, 2000 and 2500m/s. The authors found that the obliquity angle (60º) and velocity of the plates had the highest impact on the fragmentation of the projectile. Furthermore, Liden *et al*. revealed that the forward moving plate (rear plate of ERA moving in the projectile direction) had the main role in the deflection and further fragmentation of the projectile (Lidén *et al*. 2011, 2012).

In their later study Liden *et al*. found through simulations that the sliding velocity of the plate in opposite direction to the projectile must be as slow as possible in order to reach the maximum fragmentation of the projectile (Lidén and Helte 2016). Despite of its effectiveness, the ERA has an inherent danger to anyone near the protected vehicle (Yaziv *et al*. 1995, Held 2005). Therefore, another type of reactive armor has been developed without explosions, called non-explosive reactive armor (NERA) (Gov *et al*. 1992).

The non-explosive reactive armor employs a similar sandwich structure with elastomers or polymers in the middle layer. Upon impact, the middle layer due to a relatively slower shock wave prorogation will cause a rapid deformation (bulging) of the side steel plates shifting the impact

point and increasing the effective thickness, which can also destabilize the projectile. The NERA is lighter and safer while it is generally considered as less effective compared to the ERA of the same size (Fraś 2021b). Similar to ERA the non-explosive reactive armor geometry modeling consists of determining the effective obliquity and thickness of the plates embedding the elastic material.

Rosenberg and Dekel (1998) performed 2-D simulations of bulging armor. In their work, the factors affecting the bulging process were investigated and some suggestions for better performance were given. Plate thickness, intermediate layer thickness, yield strength and modulus of elasticity were varied to evaluate the performance of the bulging armor. The conclusions of their work are that the material of the intermediate layer should have low strength with a density in the range of 1.5 - 2.5 g/cm3. It was stated that the shear modulus of the intermediate layer does not affect the bulging performance. On the other hand, it was mentioned that the bulging velocity of the metal plates depends on the thickness of the intermediate layer. Rosenberg and Dekel (1998) suggested that the thicknesses of metal plates should be taken asymmetrically for a better performance.

2.2 Geometry optimization

Genetic algorithms are widely used in geometry optimization. The algorithm is inspired by Charles Darwin's theory of natural evolution and reflects the process of natural selection where the fittest individuals are selected for reproduction in order to produce offspring of the next generation. Giguère and Selig (2000) studied the multi-objective geometry optimization of blades of wind turbines using PROPGA genetic algorithm, designed for blade geometry. Blade designs having a large fitness according to the objective function for the optimization process (maximum energy capture, minimum cost of energy, etc.) have a larger probability to "reproduce" in creating the new generations compared to those with a small fitness value. A binary string represents each candidate blade geometry, and the reproduction process involves crossover and mutation operators. PROPGA uses PROPID as its analysis tool. Therefore, PROPGA has the same inverse design capabilities of PROPID (Selig and Coverstone-Carroll 1996) (Giguère and Selig 1997) (Goetz *et al*. 2012). Taking the parameters: chord, twist, blade pitch, rotor diameter, airfoil family, number of blades for the optimization, the authors determined the minimum energy cost blade geometry.

Artificial neural networks found an application in deformation detection in many fields. In the research of Gajewski *et al*. (2017), the Finite Element Method combined with Artificial Neural Network (FEM-ANN) approach was used in order to minimize the weight of air structure elements in aircraft. The authors exploited the data obtained from FEM results in ANN model for the prediction of stiffness, deformation, weight. The obtained results showed high accuracy and allowed to achieve the minimum required weight for the structure to be stiff enough not to fail.

Direct methanol fuel cells (DMFC) are a subcategory of proton-exchange fuel cells, which is used in technology that requires generation of small amounts of power for longer period of time, such as forklifts, tuggers, and mobile phone and digital cameras. Flipsen and Spitas (2011) studied the topology optimization of DMFC, using evolutionary second-order model algorithm written in Mathematica, for optimization of volume and components placement in 3D. This algorithm was applied after the optimization with the first-order heuristic model, in order to improve accuracy. The second-order algorithm relies on the best choice of components database of DMFC, that is commercially available. The authors chose translation and rotation of the objects with respect to each other, as the design parameters and optimized the DMFC weight, volume, and cost.
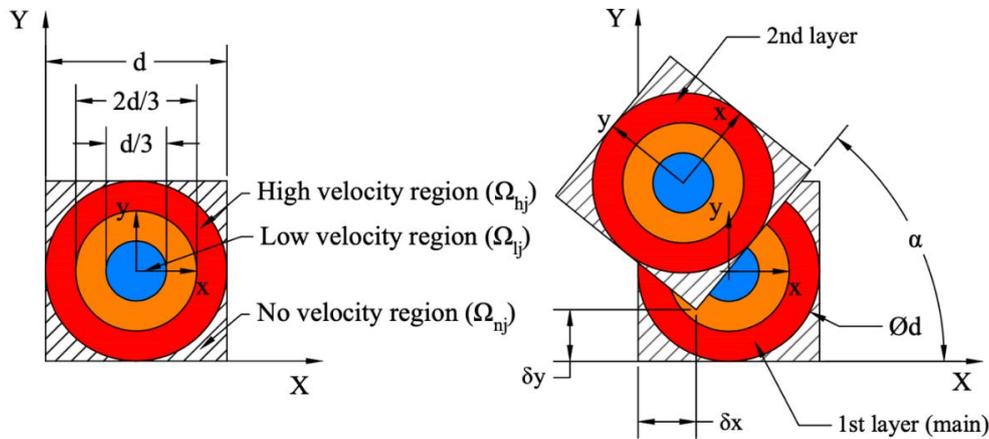
Fig. 2 Disc element in the double-layered armor: (a) velocity regions; (b) relative position between two layers

3. Description of study

3.1 Optimization objectives

As seen in the Fig. 2a, the disc element is divided into 4 regions for each layer j (j=1, 2 for the double layer armor): high velocity region (Ω_{hj}), low velocity region (Ω_{lj}), no velocity region (Ω_{nj}), and medium velocity region. The high velocity region (Ω_{hj}), is defined as a ring region from the edge of the disc to two-third of the disc diameter (d). The low velocity region (Ω_{lj}), is defined as a circular region from one-third of the disc diameter (d) to the center of the disc. The no velocity region (Ω_{nj}), is defined as the gap region not occupied by the disc in the steel case. The medium velocity region is not used for optimization since the impact occurred in this region is expected to be good. In order to maximize the tangential velocity at the point of impact, three variables for the optimization were identified:

Average tangential velocity ratio (v'_{avg}) over the entire protection area. The actual tangential velocity at any point of the layer j can be calculated as $V_j = \omega r$ or $V_j = 0$ for the no velocity region, where r is the distance from the point on the disc to the center of the disc and ω is the angular velocity of the disc. Then, the average tangential velocity (v_{avg}) and average tangential velocity ratio (v'_{avg}) can be calculated as:

$$v_{avg} = average\{\max(v1, v2)\} \tag{1a}$$

$$v'_{avg} = 2v_{avg}/(\omega d) \tag{1b}$$

where, $v1, v2$ are the tangential velocities for layer 1 and layer 2 respectively, and ω is the rotational speed. High tangential velocity area ratio (A_h) is defined as area of the high velocity regions on either of each layer divided by the whole considered area A:

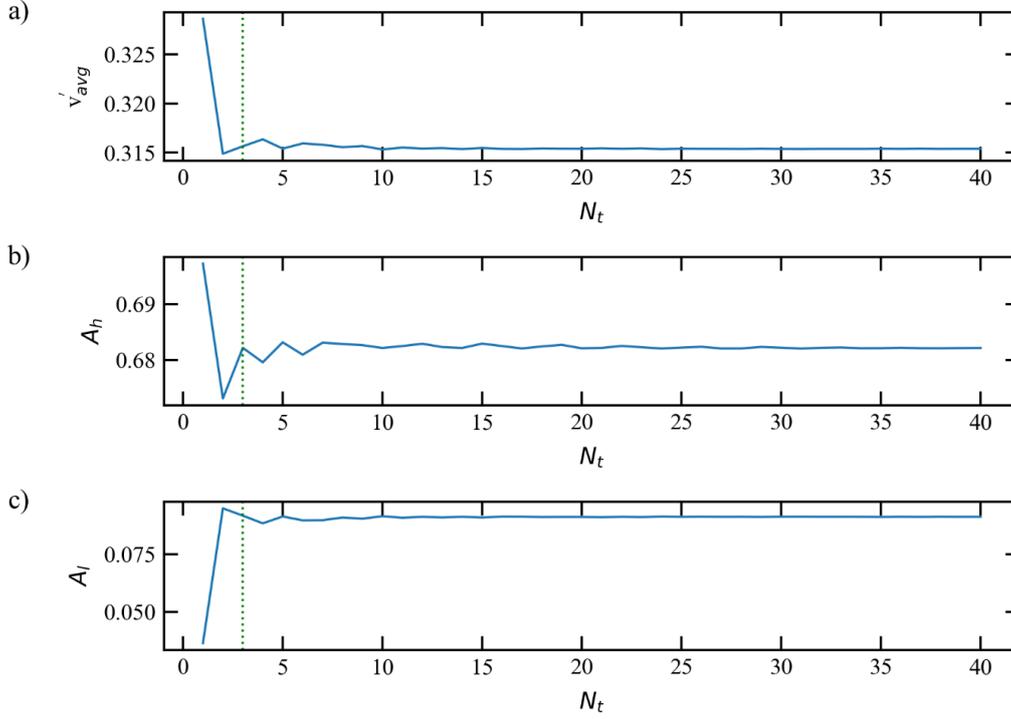$$A_h = Area\,(\Omega_{h1}) \cup Area\,(\Omega_{h2})/A \tag{2}$$

Fig. 3 Dependence of the variables on the number of tiles in a layer

Low tangential velocity area ratio (A_l) includes the area of low velocity and no velocity regions and divided by the whole considered area A:

$$A_l = (Area\,(Area\,(\Omega_{l1}) \cup Area\,(\Omega_{n1})) \cap (Area\,(\Omega_{l2}) \cup Area\,(\Omega_{n2}))/A \qquad (3)$$

The optimization objectives are: (1) maximize average tangential velocity ratio (v'_{avg}); (2) maximize high tangential velocity area ratio (A_h); and (3) minimize low tangential velocity area ratio (A_l).

3.2 Calculation of design objectives

The relative positions translation (δ_x and δ_y) and rotation (α), between the first and the second layers are considered to achieve the optimization objectives (Fig. 2b). The 1st layer of the armor (main layer) with the disc diameter of d is considered as fixed and consists of a square array (N_t x N_t) of discs. A sensitivity study of the N_t on the objective functions is conducted. As shown in Fig. 3, the objective functions are converged after N_t is larger or equal to 3 (indicated as vertical trend lines). Therefore, the square 3 x 3 array is used for the 1st fixed layer in this study in order to save the computation time in addition. The considered protected 1st layer area (A) is equal to 3d x 3d (refer to Fig. 1b).

The 2nd layer will be occupied by an array of discs to completely cover the 1st layer. The array of discs in the 2nd layer will then be displaced in x and y directions through rigid body translations and be rotated around z axis (out-of-plane axis) relative to 1st layer through a rigid body rotation

(see Fig. 2b). The displacements in x and y directions are defined as δ_x and δ_y (see Fig. 2b), respectively. The rotation around z axis is defined as α. Due to the symmetry, the range of the δ_x and δ_y is set from 0 to d/2 and the range of the α is set from 0° to 45°.

These parameters are calculated using the classification into the regions described earlier, that identify the region where a considered point (X, Y) lies. The same notation for a point and the axes in global (X, Y) and local (x, y) coordinates is used.

Using the local axes (x, y) of each layer shown on Fig. 2b, the distance (eqn. 4a) between the point and origin will simplify the classification conditions. In order to move from the global (X, Y) to local (x, y) axes, rotation by α (eqn. 4c) and displacement (eqn. 4b) are required. Then the considered point in local axes will lie in [0, d/2] x [0, d/2] domain.

Then, the distance from the center of the disc will be calculated using the given in global coordinates (X, Y) as:

$$r = \sqrt{x^2 + y^2} \tag{4a}$$

$$(x\ y) = (x_{rot} - \lfloor x_{rot}/d \rfloor \cdot d\ \ y_{rot} - \lfloor y_{rot}/d \rfloor \cdot d) - \frac{1}{2}(d\ d) \tag{4b}$$

$$(x_{rot}\ y_{rot}) = (\cos\alpha\ -\sin\alpha\ \sin\alpha\ \cos\alpha)\ X - \delta_x\ Y - \delta_y \tag{4c}$$

The region where the given point lies is identified depending on the distance from the center r:

$$\Omega_h, \text{ if } r \geq 2d/3 \text{ and } r \leq d/2 \tag{5a}$$

$$\Omega_l, \text{ if } r < d/3 \tag{5b}$$

$$\Omega_n, \text{ if } r > d/2 \tag{5c}$$

Then using this region classification v'_{avg}; is found using the expression for v' of a point:

$$v'_{avg}(\delta_x, \delta_y, \alpha) = \frac{1}{A} \int_0^{3d} \int_0^{3d} v(x, y, \delta_x, \delta_y, \alpha)\ d_x d_y \tag{6a}$$

$$v'(x, y) = \max(v'_1, v'_2) \tag{6b}$$

$$v'_j(\text{x, y, } \delta_x, \delta_y, \alpha) = \{0, if\ (x,y)\ \epsilon\ \Omega_n 2r/d, \text{ otherwise}\} \tag{6c}$$

To define the high velocity area ratio:

$$A_h(\delta_x, \delta_y, \alpha) = \frac{1}{A} \int_0^{3d} \int_0^{3d} I_h(x, y, \delta_x, \delta_y, \alpha) dxdy \tag{7a}$$

$$I_h(x, y) = \max(I_{h1}, I_{h2}) \tag{7b}$$

$$I_{hj}(\text{x, y, } \delta_x, \delta_y, \alpha) = \{1, if\ (x,y)\ \epsilon\ \Omega_{hj}, 0\text{ otherwise}\} \tag{7c}$$

Similarly, the low velocity area ratio:

$$A_l(\delta_x, \delta_y, \alpha) = \frac{1}{A} \int_0^{3d} \int_0^{3d} I_l(x, y, \delta_x, \delta_y, \alpha) dxdy \tag{8a}$$

$$I_l(x, y) = \min(I_{l1}, I_{l2}) \tag{8b}$$

$$I_{lj}(x, y, \delta_x, \delta_y, \alpha) = \{1, if(x, y)\ \epsilon\ \Omega_{lj}\ \cup\ \Omega_{nj}\ 0, othewise\} \tag{8c}$$

Since the integrands in the equations 6a, 7a, and 8a are piecewise-linear, according to the Gaussian quadrature rule approximate value of line integral is:

$$\int_a^b f(x)dx = \frac{b-a}{2} \int_{-1}^1 f(\frac{b-a}{2} x + \frac{a+b}{2}) \, dx = \frac{b-a}{2} \int_a^b f(\xi)d\xi = \frac{b-a}{2} w_i f(\xi_i) \tag{9}$$

where w_i weights of quadrature formulas and ξ_i are the quadrature points.

The Gaussian quadrature rule allows to obtain an exact result for polynomials of order 2n-1 integration. In other words, if polynomial is linear then two Gaussian weights are sufficient to get exact solution of integral. For quadratic function, it is sufficient to use three quadrature points. Gaussian quadrature points and their weights are shown in Table 1.

As shown in work (Schaal *et al*. 2015), to calculate double integrals it is easy to use Gaussian rule in the following form:

$$\int_{-1}^1 \int_{-1}^1 f(x,y)dxdy = f(x_i, y_j) w_i w_j \tag{10}$$

Then the integrals (6a, 7a, 8a) are calculated using the Gaussian quadrature rule with a negligible error.

3.3 Optimization procedure

Maximization of v'_{avg} is the main mechanism of the projectile deflection. Maximization of A_h and minimization of A_l will reduce the probability of a projectile hitting at regions with low velocities.

The "scipy" library of the "python" programming language allows optimization of the given functions. At first, each of the parameters are optimized and at last combined case is considered. At considering each parameter separately the function f $(\delta_x, \delta_y, \alpha)$, that is minimized further is:

$$-v'_{avg}(\delta x, \delta y, \alpha), - A_h(\delta_x, \delta_y, \alpha), A_l(\delta x, \delta y, \alpha) \tag{11}$$

Since the solver allows to minimize only one function (f), the weights for each objective function must be introduced based on the priority level in the optimization for the combined case.

$$f(\delta_x, \delta_y, \alpha) = -w_1 v'_{avg}(\delta_x, \delta_y, \alpha) - w_2 A_l(\delta_x, \delta_y, \alpha) \tag{12}$$

Since the values of the integrals highly differ from each other the weights are necessary to equalize them. Consider 100 random cases of placement of the second layer and calculate the

Table 1 Gaussian quadrature points

Number of points	Points, ξ_i	Weights, w_i
1	0	2
2	$+\sqrt{1/3}$	1
3	0	$\frac{8}{9}$
	$\pm\sqrt{3/5}$	$\frac{5}{9}$

Table 2 Parameter values for one layer IRA

v'_{avg}	A_l, %	A_h, %
0.2618	30.38	43.38

Table 3 Armor design for the maximum value of v'_{avg}

α	$(\delta x, \delta y)$	$v'avg$	A_l, %	A_h, %
0°	(0.5, 0.125)	0.3811	5.002	75.7

integrals separately and take the mean values of them. For v'_{avg} the mean value was 0.36, high velocity region was 0.6854, and low velocity region was 0.0895. Then the weights are equal to: w1=1.9, w2=1, w3=7.6.

Using Nelder-Mead optimization algorithm the function f is minimized. The optimization is considered converged when the incremental error is less than 0.5%. The algorithm's main advantage is its independence to the gradient of the cost function or any approximation, which means that it is applicable to non-differentiable functions or to cases where the gradient is unknown. Nevertheless, the algorithm needs to evaluate more points, becoming more time-consuming. Another disadvantage is that near local minima, the algorithm may enter in oscillation, not converging to a single value. Although it has its disadvantage in being time consuming since the algorithm needs to evaluate more points, it can yield a reasonable result for the parameters considered in this study.

4. Results & discussions

A single layered IRA with 3 by 3 tiles is chosen as the benchmark for the study, for which the parameter values are shown on Table 1 & Table 2. Al is apparently close to Ah which leads to higher probability of penetration by a projectile, since almost half of the armor can not provide high tangential velocity at the point of the impact. The unprotected regions must be covered and overall tangential velocity in the armor must increase significantly with the addition of the second layer of the IRA.

4.1 Maximization of average tangential velocity

In the Fig. 4, it is shown that the largest and smallest values of v'_{avg} are obtained at α=0°. The smallest value at that angle is explained by overlapping of two layers as seen in Fig. 5a, when the displacements are small, and the double layered IRA behaves as a single layered. Moreover, the values of the parameter are larger when the tile corner of the second layer is placed at the center of a side of the tile from the first layer. The largest values of v'_{avg} are obtained at $d_x=d_y=0.125d$ while the smallest values are found at $d_x=d_y=0$, where two layers of the disc are stacked on top each other. At angles of placement larger than 10° the variance of the values of the parameter drops significantly and keeps narrow up to 45°.

Fig. 5 shows the contour plot of how v'_{avg} distribution changes with the placement angle of the second layer until 10°. The concentration of large values shifts towards the center of the first quarter [0, 0.5d] x [0, 0.5d] of the main layer tile. The maximum value of v'_{avg} is obtained at
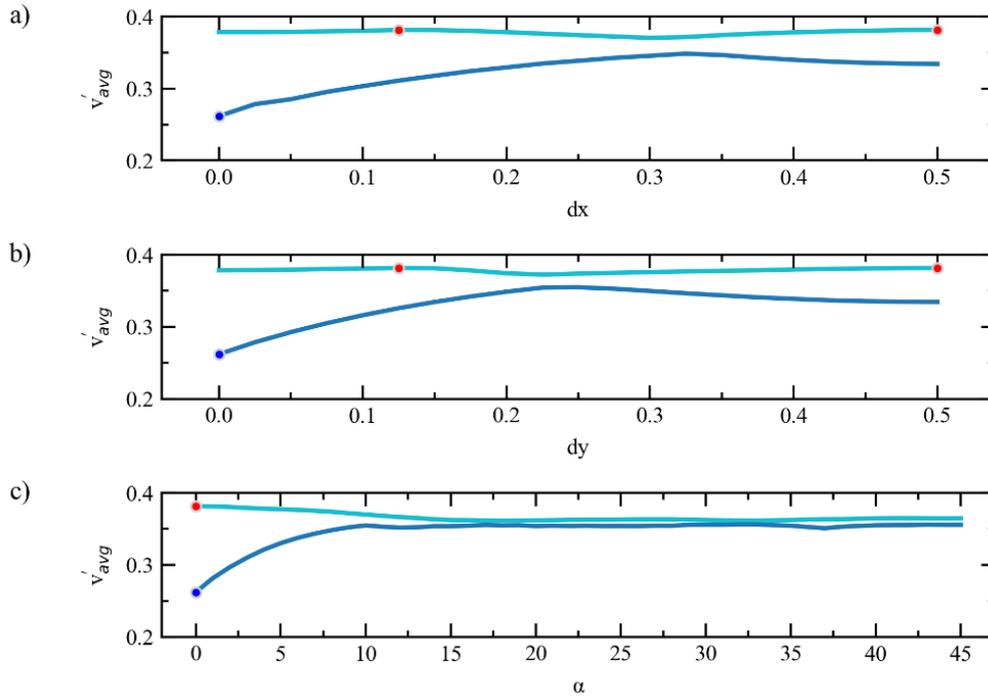
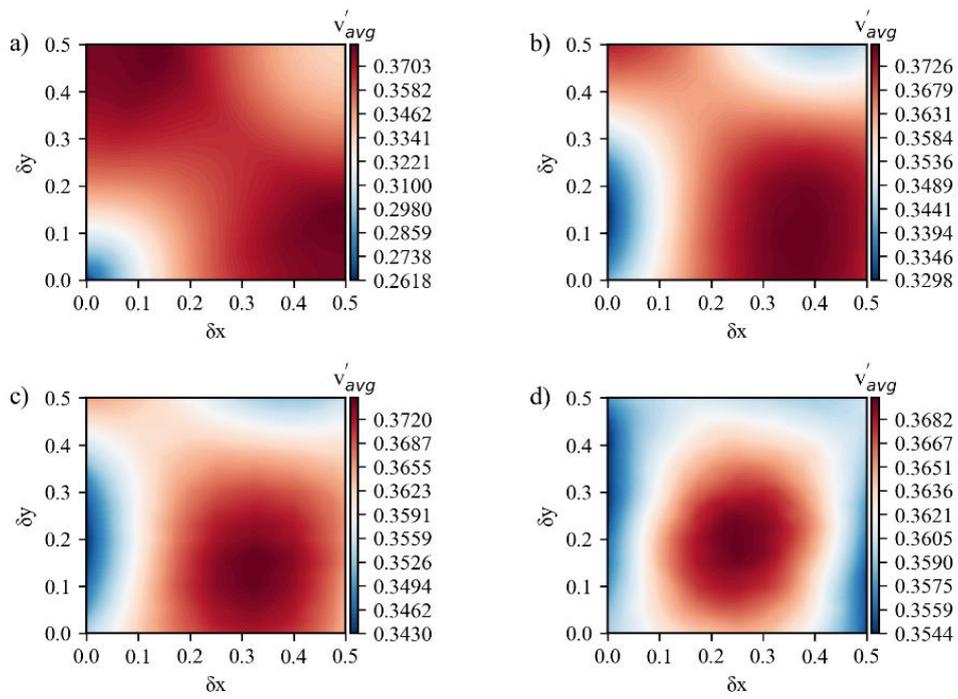Fig. 4 Maximum and minimum values of v'_{avg} at different parameters

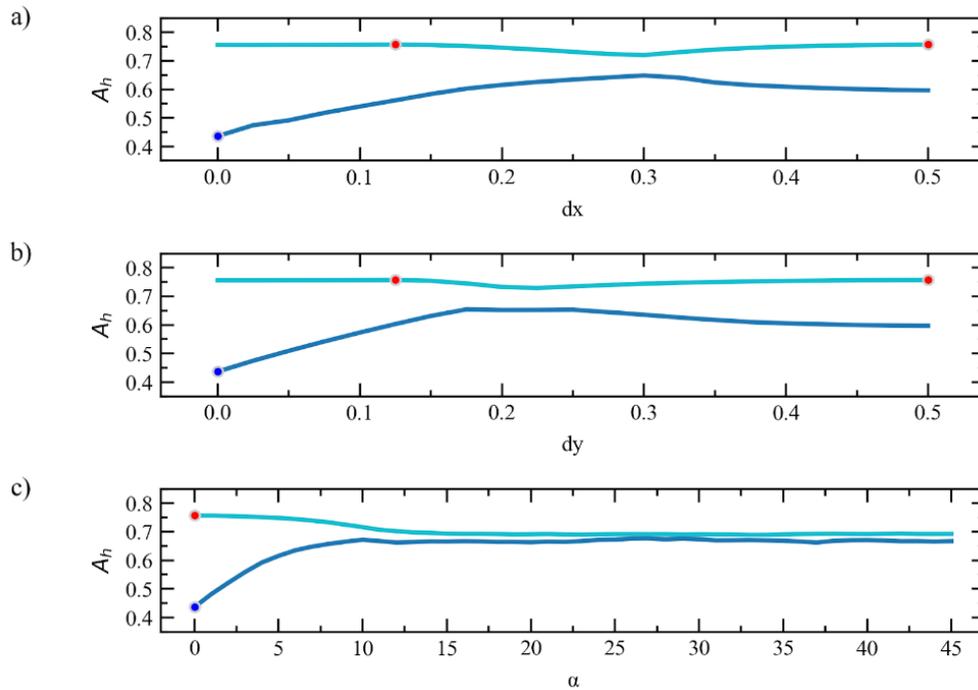Fig. 5 Contour plots of v'_{avg} at angles of placement: a) 0º, b) 5º, c) 7º, d) 10º

Fig. 6 Maximum and minimum values of A_h at different parameters

Table 4 Armor design for the maximum value of A_h

α	$(\delta x, \delta y)$	$v'avg$	A_l, %	A_h, %
0°	(0.5,0.125)	0.3811	5.002	75.7

right bottom corner side as shown in the Table 3. Accordingly, the average distance from a disc center is 38.11% of the disc diameter and the projectile has 5.002% probability penetrating the disc as seen from A_l. The layout showed 75.7% coverage of the high velocity area.

4.2 Maximization of high tangential velocity area

Figs. 6 and 7 show the variance of high tangential velocity area over the study parameters, which shows a similar trend as the average tangential velocity. It is observed that, the placement position of the tile $(\delta x, \delta y)$, at which the average tangential velocity was maximum, A_h also reached the largest as expected, covering the low velocity region in the 1st layer by the 2nd layer. At the value of $\alpha=0°$, the high velocity region covers most of the spaces, which is consistent with the average tangential velocity. The highest A_h is observed at a placement of $d_x=0.5$ and $d_y=0.125$ as shown in Table 4, which results in: $v'avg = 0.3811$ and $A_l = 5$ %.

4.3 Minimization of low tangential velocity area

Figs. 8 and 9 show the variance of low tangential velocity area over the study parameters.

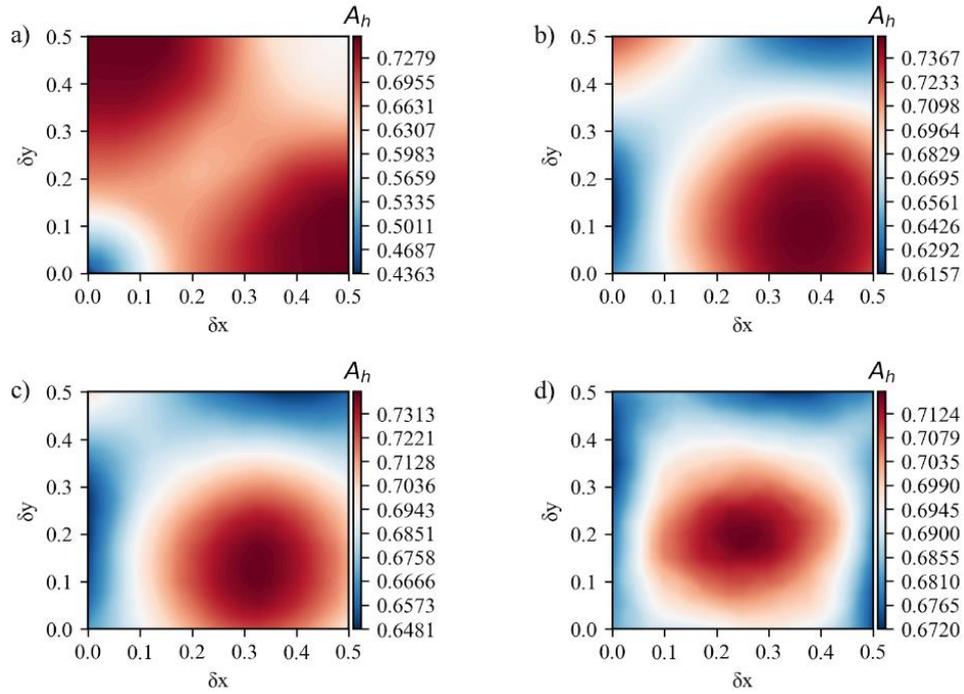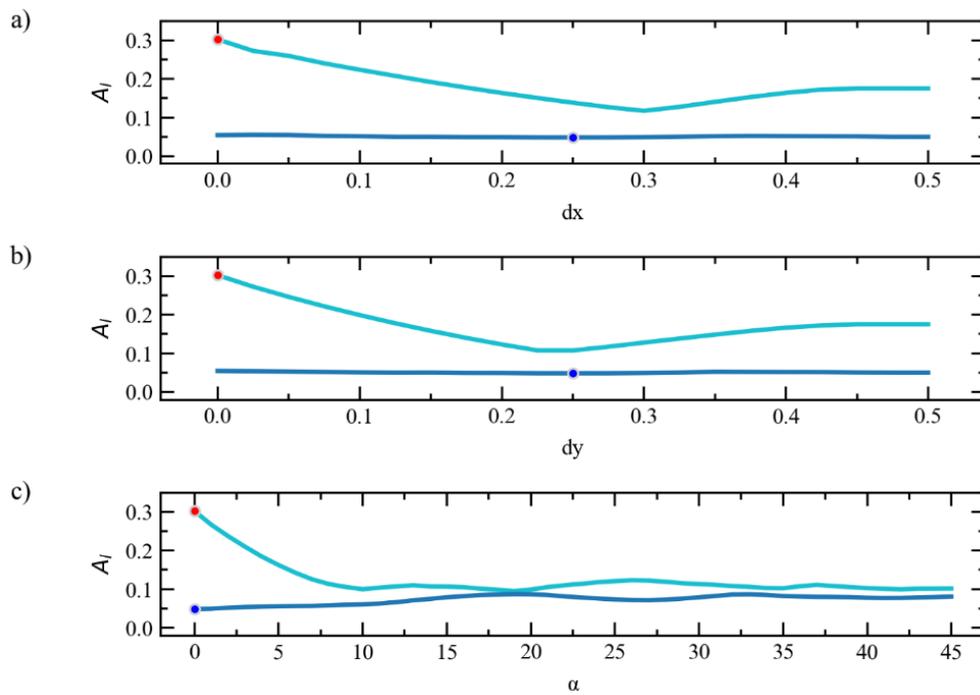Fig. 7 Contour plots of A_h at angles of placement: a) 0º, b) 5º, c) 7º, d) 10º

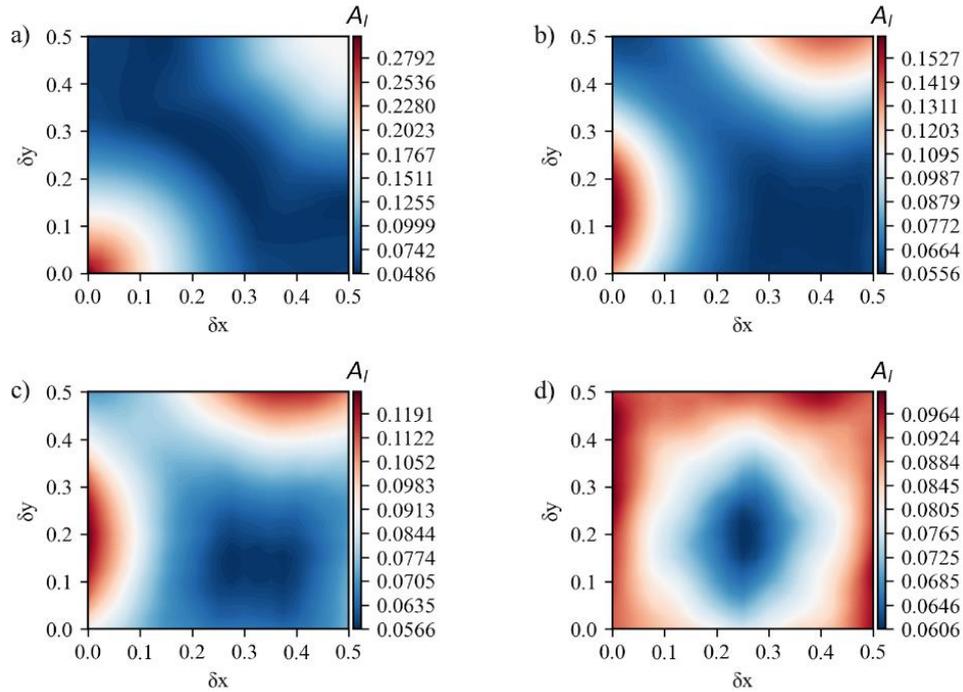Fig. 8 Maximum and minimum values of A_l at different parameters

Fig. 9 Contour plots of A_l at angles of placement: a) 0º, b) 5º, c) 7º, d) 10º

Table 5 Armor design for the minimum value of A_l

α	(δx, δy)	$v'avg$	A_l, %	A_h, %
0º	(0.25, 0.25)	0.363	4.03	65.43

Table 6 Armor design for combined optimal targets

α	(δx, δy)	$v'avg$	A_l, %	A_h, %
2.6º	(0.455, 0.133)	0.3719	4.2	74.3

Following the same reasons as $v'avg$, the low velocity area ratio shows lowest values at 0º as seen in Fig. 8. The smallest value of 4.03% was obtained at the same 0º angle of placement since the largest value of $v'avg$ was obtained at that angle of placement. Increasing the angle of placement reduces the maximum value of the A_l in the domain of (δx, δy) until 10º after which oscillates around a fixed value. The lowest A_l is observed at a placement of $d_x=d_y=0.25$ as shown in Table 5, which results in: $v'avg = 0.363$ and $A_h = 65.43$ %. These values are slightly less than the maximum values observed in Sections 4.1 and 4.2.

4.4 Multi-objective optimization

Table 6 shows the results of the combined optimization process. The optimization process involves a trade-off between these three objectives, as increasing $v'avg$ and A_h will often lead to an increase in A_l. Therefore, finding a balance between these objectives is essential to achieve the

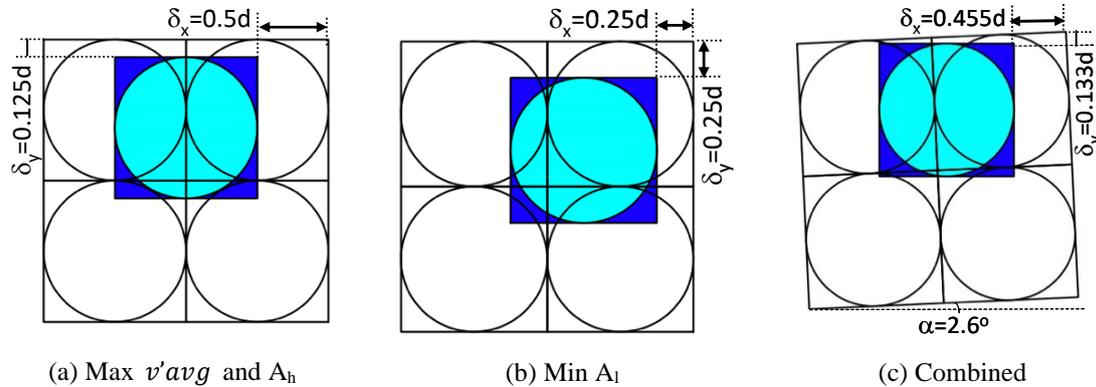(a) Max $v'avg$ and A_h (b) Min A_l (c) Combined

Fig. 10 Optimal layouts for one tile of the main layer (colored)

best possible overall solution (Kaveh and Bakhshpoori 2016). In this case, the optimization process has led to a solution where the maximum values for $v'avg$ and A_h have been achieved, while still achieving a minimum value for A_l at 4.2% close to its minimum of 4.03%. This solution represents the best possible compromise between the conflicting objectives and can be considered a Pareto-optimal solution. Overall, multi-objective optimization is a powerful tool that can help to find the best possible solution when dealing with multiple objectives that conflict with each other. By optimizing these objectives simultaneously, it is possible to find a balance between them and achieve the best possible overall solution. The final optimal positions of two layers of armors are shown in Fig. 10: (a) maximizing V_{avg} and A_h, (b) minimizing A_l; and (c) combined optimal.

5. Conclusions

This paper presents a geometry optimization study for a doubled-layer armor with rotating discs. Since the key concept of the rotating disc armor is to achieve large tangential velocity at the point of impact to deflect the high-speed projectile, it is important to maximize the average tangential velocity, maximum the high tangential velocity region, and minimize the low tangential velocity region on the armor surface. The optimization was achieved by a double-layer configuration with the 2nd layer displacing and rotating from the 1st layer. The following conclusions can be made from the study:

1. The single layer armor has a relatively small high-velocity but large low-velocity region, which will reduce the effectiveness of the rotating disc concept.

2. The optimal design for the maximum average tangential velocity and the high velocity region occurred at the same configuration where the 2nd layer is displaced from the 1st layer in x direction by 0.5d and in y direction by 0.125d without rotation.

3. The optimal design for the low velocity region occurred when the 2nd layer is displaced from the 1st layer in x direction by 0.25d and in y direction by 0.25d without rotation.

4. The combined optimal design occurred when the 2nd layer is displaced from the 1st layer in x direction by 0.455d and in y direction by 0.133d without a rotation of 2.6 degree. This design can increase $v'avg$ by 38%, increase A_h by 71.3%, and reduce A_l by 86.2% as compared to the single layer configuration.

5. The number of discs in one layer does not significantly affect the optimized design when this number exceeds a certain threshold of 3x3 discs.

6. The combined optimal design cannot eliminate the low velocity region, which will affect the effectiveness of the rotating disc armor. Therefore, the optimal design might be further improved with arbitrary placement of the tiles, including the shape of the tile which can be for instance hexagon shaped. This design concept requires a follow-up study.

Acknowledgments

References

Boorla, S.M., Bjarklev, K., Eifler, T., Howard, T.J. and McMahon, C.A. (2019), "Industry 4.0-A challenge for variation simulation tools for mechanical assemblies", *Adv. Comput. Des.*, **4**, 43-52. https://doi.org/10.12989/acd.2019.4.1.043.

Cohen-Arazi, Y., Sokol, E., Frilling, S. and Shaked, I. (2012), "Extremely insensitive detonating substance and method for its manufacture", *United States Patent*, 8277584 B2.

Fras, T. (2021a), "Experimental and numerical study on a non-explosive reactive armour with the rubber Interlayer applied against kinetic-energy penetrators—the 'bulging effect' analysis", *Materials*, **14**. https://doi.org/10.3390/ma14123334.

Fraś, T. (2021b), "Modelling of bulging steel-elastomer armour applied against long-rod projectiles", *J. Phys.*, **1855** (1), 012-016. https://doi.org 10.1088/1742-6596/1855/1/012016.

Flipsen, S. and Spitas, C. (2011), "Direct methanol fuel cells: A database-driven design procedure", *J. Power Sources*, **196**, 8472-8483. https://doi.org/10.1016/j.jpowsour.2011.06.014/

Gajewski, J., Golewski, P. and Sadowski, T. (2017), "Geometry optimization of a thin-walled element for an air structure using hybrid system integrating artificial neural network and finite element method", *Compos. Struct.*, **159**, 589-599. https://doi.org/10.1016/j.compstruct.2016.10.007.

Giguère, P. and Selig, M. (1997), "Aerodynamic Blade Design Methods for Horizontal Axis Wind Turbines", *Proceedings of the 13th Canadian Wind Energy Conference*, Quebec City, Quebec, Canada.

Giguere, P. and Selig, M. (2000), "Blade geometry optimization for the design of wind turbine rotors", *Proceedings of the 2000 ASME Wind Energy Symposium*. https://doi.org/10.2514/6.2000-45.

Goetz, J., Tan, H., Renaud, J. and Tovar, A. (2012), "Two-material optimization of plate armor for blast mitigation using hybrid cellular automata", *Eng. Optimiz.*, 985-1005. https://doi.org/10.1080/0305215X.2011.624182.

Gordini, M., Habibi, M.R., Sheidaii, M.R. and Tahamouliroudsari, M. (2017), "Reliability analysis of double-layer domes with stochastic geometric imperfections", *Adv. Comput. Des.*, **2**(2), 133-146. https://doi.org/10.12989/acd.2017.2.2.133.

Gov, N., Kivity, Y. and Yaziv, D. (1992) "On the interaction of a shaped charge jet with a rubber filled metallic cassette", *Proceedings of the 13th International Symposium on Ballistics*, 95-102.

Graswald, M., Gutser, R., Breiner, J., Grabner, F., Lehmann, T. and Oelerich, A. (2019), "Defeating Modern Armor and Protection Systems", *Hypervelocity Impact Symposium*, **4**. https://doi.org/10.1115/HVIS2019-050.

Held, M. (1973), "Schutzeinrichtung gegen Geschosse, insbesondere Hohlladungsgeschosse (protection device against projectiles, especially shaped charges)", *Germany Patent*, 2358227.

Held, M. (2005), "Defeating mechanisms of reactive armour sandwiches", *Proceedings of the 22nd*

International Symposium on Ballistics, 1001-1007.

Kaveh, A. and Bakhshpoori, T. (2016), "An efficient multi-objective cuckoo search algorithm for design optimization", *Adv. Comput. Des.*, **1**(1), 87-103. http://dx.doi.org/10.12989/acd.2016.1.1.087.

Lanz, W., Odermatt, W. and Weihrauch, G. (2001), "Kinetic energy projectiles: development history, state of the art, trends", *Proceedings of the 19th International Symposium on Ballistics*, Interlaken, Switzerland, May, 1191-1197.

Lidén, E. andersson, O. and Lundberg, B. (2011), "Deformation and fracture of a long-rod projectile induced by an oblique moving plate: Experimental tests", *Int. J. Impact Eng.*, **38**, 989-1000. https://doi.org/10.1016/j.ijimpeng.2011.07.002.

Lidén, E. and Helte, A. (2016), "The break-up tendency of long rod projectiles", *Defence Technology*, **12**, 177-187. https://doi.org/10.1016/j.dt.2016.01.003.

Lidén, E., Mousavi, S., Helte, A. and Lundberg, B. (2012), "Deformation and fracture of a long-rod projectile induced by an oblique moving plate: Numerical simulations", *Int. J. Impact Eng.*, **40-41**, 35-45. https://doi.org/10.1016/j.ijimpeng.2011.09.003.

Mayseless, M. (2011), "Effectiveness of explosive reactive armor", *J. Appl. Mech.*, **78**, 051006. https://doi.org/10.1115/1.4004398.

Mayseless, M., Ehrlich, Y., Falcovitz, Y.,Weihs, D. and Rosenberg, G. (1984), "Interaction of shaped-charge jets with reactive armor", *Proceedings of the 8th Int. Sym. on Ballistics*, Orlando, Florida.

Mayseless, M., Friling, S. and Misiuk, L. (2019), "Re-visiting the mass-flux model for explosive reactive armor and the effect of plate thickness", *Defence Technology*, **15**, 779-785. https://doi.org/10.1016/j.dt.2019.08.015.

Rosenberg, Z. and Dekel, E. (1998), "A parametric study of the bulging process in passive cassettes with 2-D numerical simulations", *Int. J. Impact Eng.*, **21**, 297-305. https://doi.org/10.1016/S0734-743X(97)00082-1.

Rosenberg, Z., Dekel, E., Ashuach, Y. and Yeshurun, Y. (2008), "On the main mechanisms for defeating AP projectiles, long rods and shaped charge jets", *Int. J. Impact Eng.*, **36**, 588-596. https://doi.org/10.1016/j.ijimpeng.2008.09.003.

Schaal, K., Bauer, A., Chandrashekar, P., Pakmor, R., Klingenberg, C. and Springel, V. (2015), "Astrophysical hydrodynamics with a high-order discontinuous Galerkin scheme and adaptive mesh refinement", *Monthly Notice. Royal Astronom. Soc.*, **453**(4), 4279-430. https://doi.org/10.1093/mnras/stv1859.

Selig, M. and Coverstone-Carroll, V. (1996), "Application of a genetic algorithm to wind turbine design", *ASME J. Solar Energy Eng.*, **118**, 22-28. https://doi.org/10.1115/1.2792688.

Yaziv, D., Friling, S. and Kivity, Y. (1995), "The interaction of inert cassettes with shaped charge jets", *Proceedings of the 15th International Symposium on Ballistics*, **1**, 461-467.

TK

Notations

d – Disc diameter
α − second layer angle of placement
(δx, δy) – Placement position of the second layer
Ω_l – low velocity region
Ω_h – high velocity region
Ω_n – no velocity region
(x, y) – coordinates of a point in local coordinates
(X, Y) – coordinates of a point in the global coordinates

r – Distance from the disc center to the given point (using (X, Y))

(x_{rot}, y_{rot}) – Rotated along z direction by - α (X, Y) coordinates

I_l – function that returns 1 if a point in both layers lies in low velocity region

I_h – function that return 1 if a point in at least one layer lies in high velocity region

I_{lj} – function that returns 1 if a point lies in low velocity region

I_{hj} – function that return 1 if a point lies in high velocity region

A_l – low velocity area ratio

A_h – high velocity area ratio

v' − tangential velocity of a point divided by angular velocity

v'_{avg} - average v' in the armor which represents the average distance from the disc center